

**Ligand-mediated electron-transport channels enhance photocatalytic  
activity of plasmonic nanoparticles**

*Gayatri Joshi<sup>†a</sup>, Rajesh Kashyap<sup>†a</sup>, Kalyani Patrikar<sup>†a</sup>, Anirban Mondal<sup>\*a</sup>, Saumyakanti  
Khatua<sup>\*a</sup>*

<sup>[a]</sup> Chemistry Discipline, Indian Institute of Technology Gandhinagar, Palaj, Gujarat-382055,  
India.

<sup>†</sup> These authors have contributed equally

**Table of Contents:**

<i>Item</i>	<i>Page No.</i>
Experimental Section	3-5
UV-visible extinction spectra of AuTP in acetonitrile	5
SEM analysis of AuTNP after functionalization with 4-Br-Ph-SH	6
LSPR spectra of ligand attached AuTP substrate before and after photocatalysis	6
SERS analysis of Br-Ph-S-AuTP/F-Ph-S-AuTP before and after photocatalysis	7
SEM analysis of Br-Ph-S-AuTP after photocatalysis.	7
Comparison of photocatalytic H <sub>2</sub> production with and without hole scavenger using 4-Br-Ph-S-AuTP	8
Schematic representation of AuTP functionalization with 2-Br-Ph-SH and 3-Br-Ph-SH	8
UV-visible extinction spectra of AuTP before and after 2-Br-Ph-SH, 3-Br-Ph-SH, and 4-Br-Ph-CH <sub>2</sub> -SH	9
SERS spectra of AuTP after 2-Br-Ph-SH, 3-Br-Ph-SH, and 4-Br-Ph-CH <sub>2</sub> -SH	9
EIS spectra of the various ligand-functionalized AuTP substrates	10
SERS spectra of 4-bromo thiophenol and the ligand-bounded AuTP substrates	10
Photocatalytic H <sub>2</sub> and O <sub>2</sub> production observed overtime for 4-Br-Ph-S-AuTP	11
Comparison of H <sub>2</sub> production observed at 32 <sup>0</sup> C, >1000nm, 808 nm, and CH <sub>3</sub> CN	11
Comparison of the H <sub>2</sub> production observed after 6hr with the 4- Br-Ph-S-AuTP at 32 <sup>0</sup> C, at 32 <sup>0</sup> C after ethanol rinsing, and under 808 nm illumination.	12
GC chromatogram measured after 6hr at 32 <sup>0</sup> C and 40 <sup>0</sup> C with 4-Br-Ph-S-AuTNP	12
Energy level diagram showing possible charge-carrier efficiency in pristine Au at 808 nm	13
Photocatalytic H <sub>2</sub> production with benzene thiol and cyclohexane thiol modified AuTP	13
Light profile of white lamp with >1000 nm LP filter	14
Table S1	15
References	16

## **Experimental section:**

**Materials:** Chloro(triethyl phosphine)gold(I) ( $\text{Et}_3\text{PAuCl}$ ), poly(methylhydrosiloxane) (PMHS, molecular weight (MW) = 1700–3300), trioctylamine (TOA), 4-bromothiophenol (4-Br-Ph-SH), 2-bromothiophenol (2-Br-Ph-SH), 3-bromothiophenol (3-Br-Ph-SH), 4-bromobenzylmercaptan (4-Br-Ph- $\text{CH}_2$ -SH), 4-fluorothiophenol (4-F-Ph-SH), 4-chlorothiophenol (4-Cl-Ph-SH), 4-nitrothiophenol (4- $\text{NO}_2$ -Ph-SH), 4-mercaptophenol (4-OH-Ph-SH), 4-methoxythiophenol (4- $\text{CH}_3\text{O}$ -Ph-SH), thiophenol (4-H-Ph-SH), acetonitrile, ethanol, methanol, isopropyl alcohol, hydrochloric acid (HCl), nitric acid ( $\text{HNO}_3$ ) were purchased from Sigma Aldrich. 30 mL borosil glass test tubes, microscope glass slides, and Silicon rubber stoppers were purchased from Supertek and used to prepare photocatalytic cells. Before use, all glass containers were pre-cleaned with aqua regia (3:1 HCl:  $\text{HNO}_3$ ) solution. Milli-Q® water was used from the Milli-Q direct water purification system from Millipore.

**Synthesis of Triangular Gold Nanoprisms:** Triangular gold nanoprisms (AuTPs) was synthesized by following a modified version of the previously published method<sup>1</sup>. In detail,  $\text{Et}_3\text{PAuCl}$  (10 mg, 1.42 mM) was dissolved in 5 mL acetonitrile solution and allowed to stir at room temperature for 5 minutes. The capping ligand TOA (90  $\mu\text{L}$ ) and the reducing agent PMHS (300  $\mu\text{L}$ ) were added to the reaction solution under stirring. The solution temperature was maintained at 40°C. The formation of AuTP was monitored via the color change of the solution, starting from colorless to pink, purple, blue, and dark blue at the end. At this point, the reaction was diluted further by adding 15 mL acetonitrile and stirred for another 60-80 minutes until the LSPR dipole peak reached 750 nm (Figure S1).

**AuTP attachment onto the glass substrate:** The glass slides were cut in 2.5X2.1 cm dimensions using a glass cutter. The coverslips were rinsed with isopropyl alcohol through 5 minutes of sonication twice. The coverslips were dried overnight in the oven before use. The freshly synthesized AuTP solution was added to the pre-cleaned dry glass coverslips for 2-2.5 hrs. The solution was removed, and the AuTP attached to the glass was rinsed with ethanol by incubating it in ethanol solution for 10-15 minutes, dried, and stored at room temperature until used for further functionalization.

**AuTP surface functionalization with different groups substituted thiophenol ligands:** The AuTP@glass substrates were incubated into the 5mM thiol ligand solution prepared in ethanol for 12 hr. The solution was removed, and the thiol functionalized substrates were rinsed with ethanol, dried, and utilized for further characterization and photocatalytic experiment.

**Photocatalysis experiment set up:** 15 mL of millipore water was added to the 30 mL of a pre-cleaned glass test tube. The thiol functionalized AuTP@glass substrate was immersed into the solution, and the test tube was sealed with the silicon rubber septum and covered with parafilm and grease. The water solution was purged with N<sub>2</sub> for 30-40 minutes to remove air oxygen from the solution. Baseline GC was measured by injecting the headspace gas before light illumination. An 808 nm CW laser (SLOC, model: IRM808TA-2000) was used as a light source. An appropriate lens (Thorlabs) was used to adjust the beam size. Laser excitation power was measured using Nova II Ophir, Newport power meter.

The incident photon to hydrogen conversion efficiency was calculated using the following equation:

$$IPHCE(\%) = \frac{(\# \text{ of Hydrogen molecule produced})}{(\# \text{ of incident photons})} \times 100$$

Where # of incident photons/hr was calculated at 808 nm with the power density of 100 mW/cm<sup>2</sup>.

**Spectroscopy and Microscopy Analysis:** Analytik Jena specord 210 plus UV-visible spectrophotometer was used to record the AuTP LSPR spectra in solution and on a glass substrate. All extinction spectra of AuTPs in solution were obtained using 0.1 mL of reaction solution diluted with 2.0 mL of acetonitrile. The extinction spectra of AuTP attached to glass substrates were collected in air background. All spectra were recorded at room temperature. Scanning electron microscopy (SEM) micrographs of TNPs attached to ITO-glass coverslips were acquired using an SEM (JSM 7600FJEOL) at 10 kV. A gas-tight leur-lock Valco syringe was used for injections into gas chromatography (GC) instrument (Dhruva CIC) with a TCD detector. The GC was calibrated with standard H<sub>2</sub> gas samples in a similar reaction condition. For the inductively coupled plasma optical emission spectrometry (ICP-OES) experiment, the AuTP-attached glass was digested into a freshly prepared 10 mL aqua-regia. After the complete digestion, 250 µL of the sample was further diluted with 10 mL of 0.2% of HNO<sub>3</sub> for the ICP-OES measurement (Model Nexion 2000B ICP-MS). The SERS was done with 785nm laser diode excitation with 10mW power with 10s laser exposure using in-situ Raman probe (Kaisar Raman rxn System).

**Theoretical Calculations:** Electronic structure calculations were based on density functional theory (DFT)<sup>2,3</sup>. To replicate the experimental conditions in simulations, the nanoparticle-

ligand systems were initially optimized for each ligand molecule on the Au surface using the Quickstep module provided by the CP2K program<sup>4,5</sup>. The surface was simulated by creating a single-layered slab with dimensions 16 Å by 14 Å, with a 10 Å vacuum in the *z*-direction, and ligand molecule arranged with S of thiol group attached to Au on the surface. This simulation stack allowed the evaluation of microscopic phenomena at the ligand-Au interface. Exchange-correlation potentials were treated within the generalized gradient approximation (GGA) employing the Perdew-Burke-Ernzerhof (PBE) functional<sup>6</sup>. The energy cutoff was set to 500 Ry for the auxiliary plane wave expansion of the charge density. Valence electrons were modeled explicitly, whereas core electrons have been treated with norm-conserving Goedecker-Teter-Hutter (GTH) pseudopotentials<sup>7,8</sup>. The Brillouin zone was integrated with a reciprocal space mesh consisting of only the gamma point. Grimme's DFT-D3 van der Waals corrections<sup>9</sup> were applied to account for the long-range dispersion forces. Further computations of ground state properties within the DFT framework were performed on this stack using the Gaussian09 program<sup>10</sup>. Basis set Def2-SVP<sup>11-14</sup> was used for all atoms. B3P86 hybrid density functional<sup>15-17</sup> was employed as the method. Orbital information was generated separately for the Au surface, ligand molecule, and the entire interface stack using IOP 3/33 as implemented in Gaussian09. Based on these outputs, the CATNIP program<sup>18</sup> was employed to obtain charge transfer integrals.

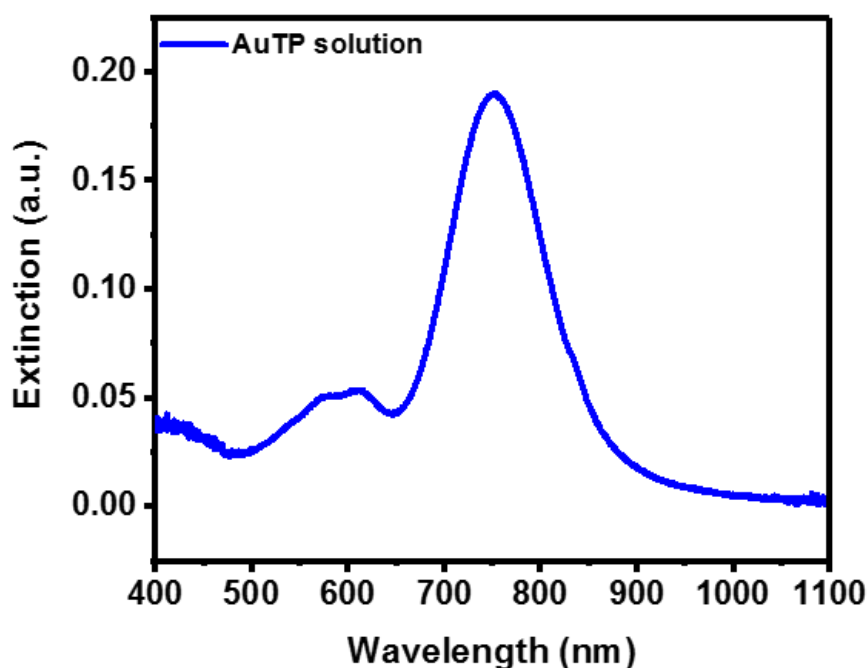


**Figure S1:** Uv-visible extinction spectra of AuTP into acetonitrile solution.

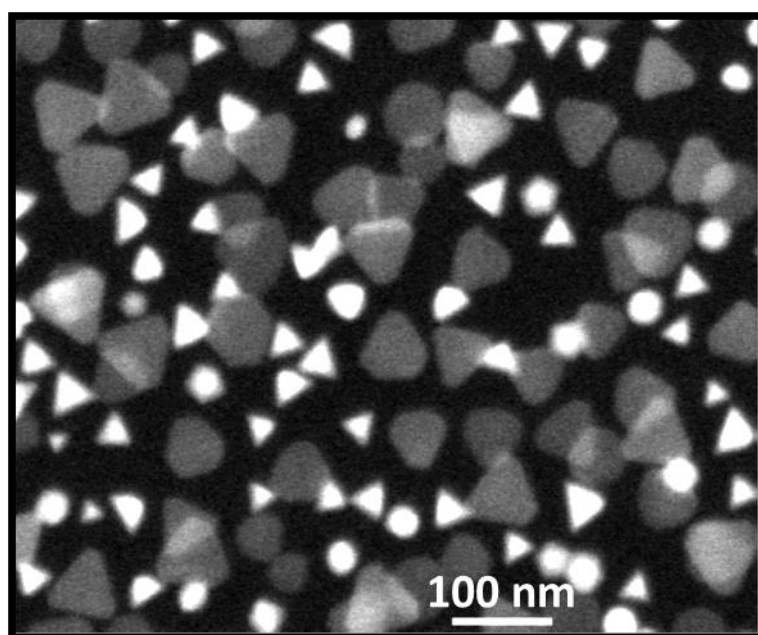


**Figure S2:** SEM analysis of AuTP after attachment of 4-Br-Ph-SH.

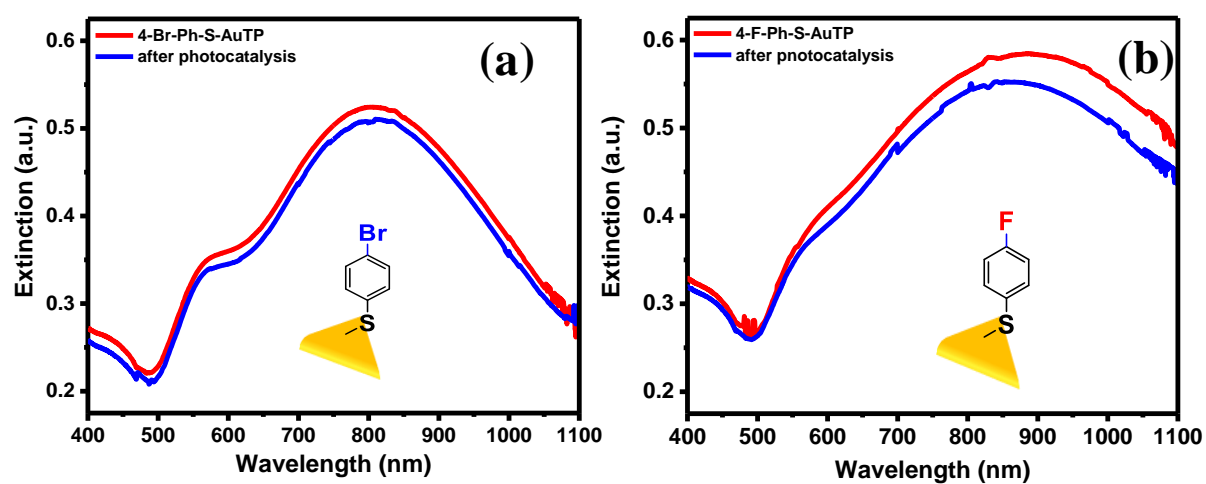


**Figure S3:** Uv-visible extinction spectra of 4-Br-Ph-S-AuTP (a) and 4-F-Ph-S-AuTP (b) substrates before (red) and after 6hr of photocatalysis (blue).

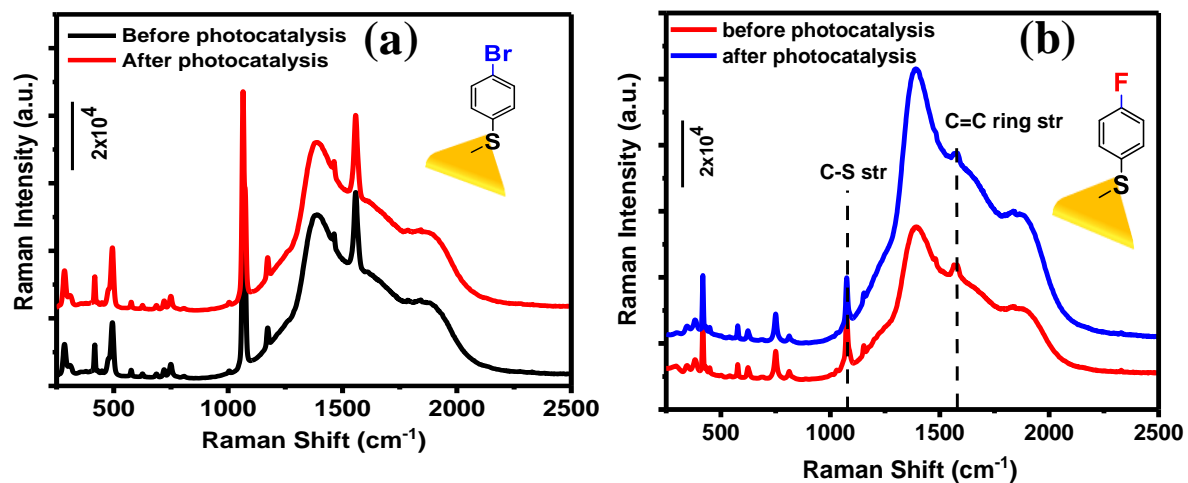


**Figure S4:** SERS spectra of 4-Br-Ph-S-AuTP (a) and 4-F-Ph-S-AuTP substrate before (red) and after 6hr of photocatalytic reaction (blue).

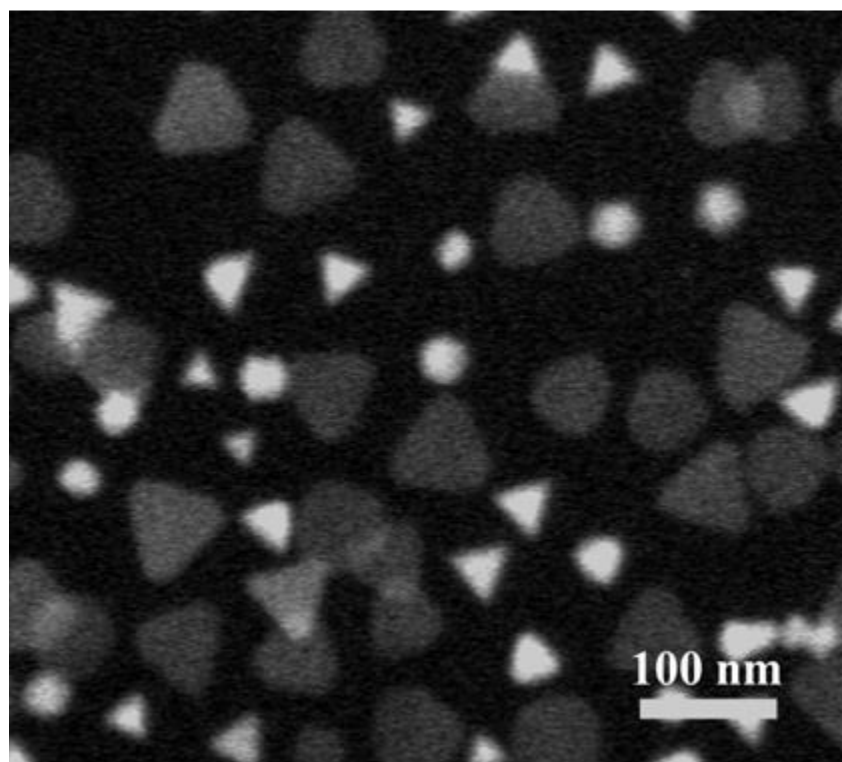


**Figure S5:** SEM image of 4-Br-Ph-S-AuTP after photocatalysis. The scale bar is 100 nm.

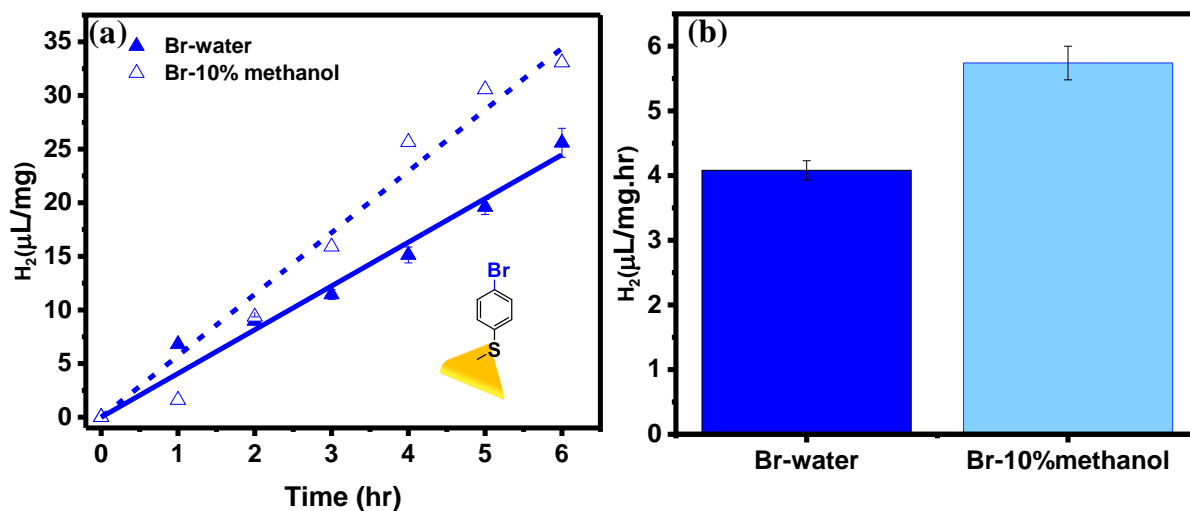


**Figure S6:** Comparison of photocatalytic H<sub>2</sub> production observed over time (a) and the HER rate (b) for 4-Br-Ph-S-AuTP substrate with and without the presence of hole scavenger (methanol).

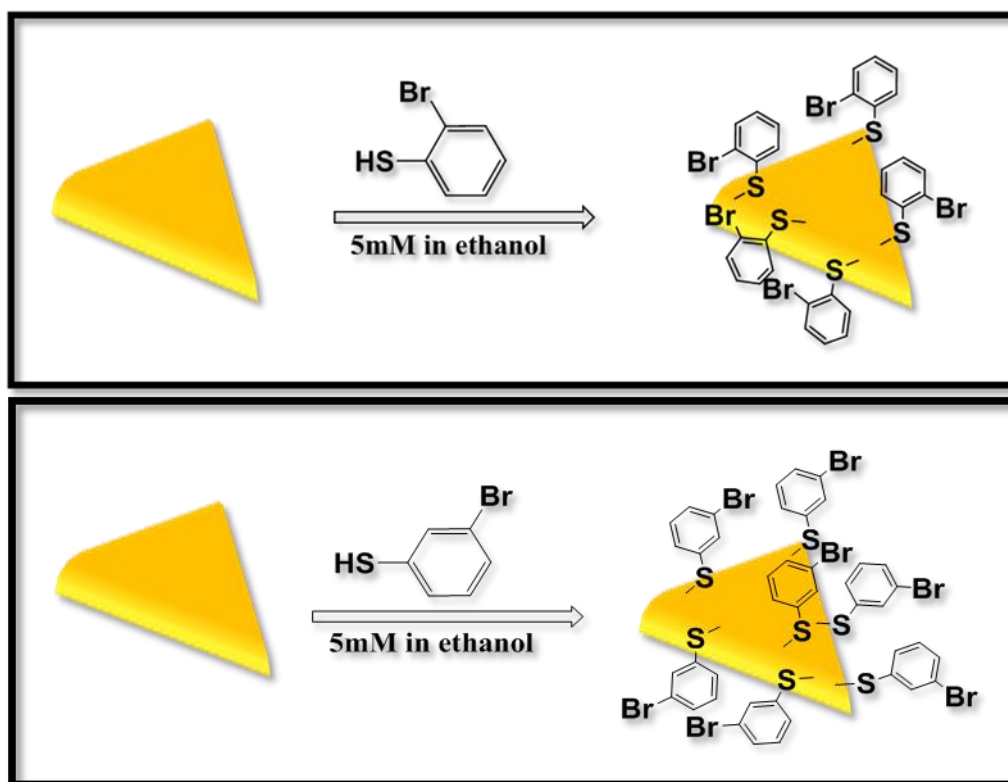


**Figure S7:** Schematic representation of the AuTP functionalization with 2-Br-Ph-SH and 3-Br-Ph-SH.

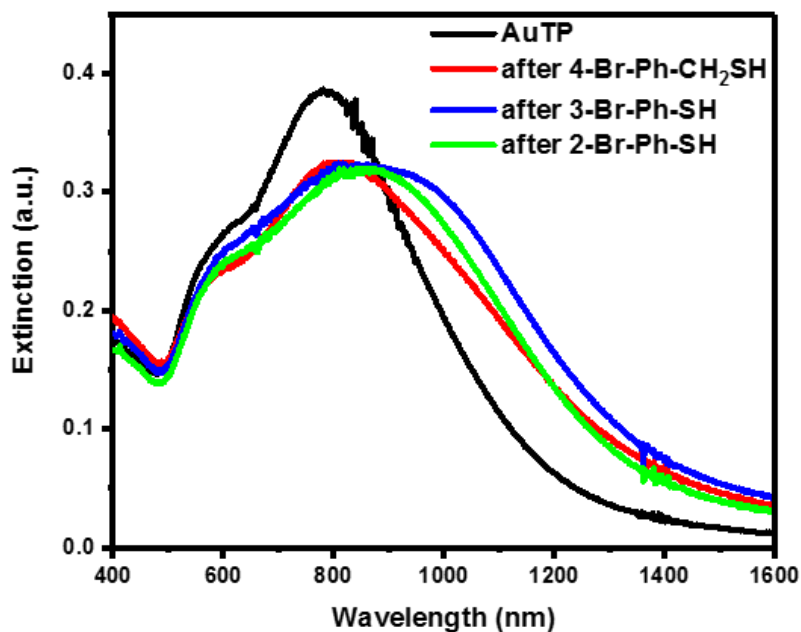


**Figure S8:** Uv-visible extinction spectra of AuTP before (black) and after functionalization with 2-Br-Ph-SH (green), 3-Br-Ph-SH (blue), and 4-Br-Ph-CH<sub>2</sub>SH (red).

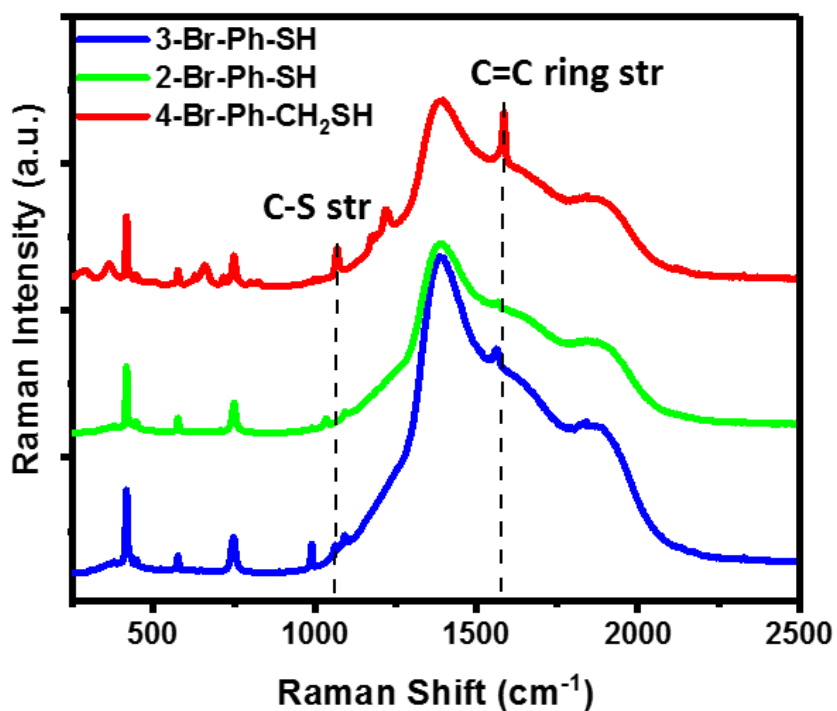


**Figure S9:** SERS spectra of AuTP substrate after functionalization with 2-Br-Ph-SH (green), 3-Br-Ph-SH (blue), and 4-Br-Ph-CH<sub>2</sub>SH (red).

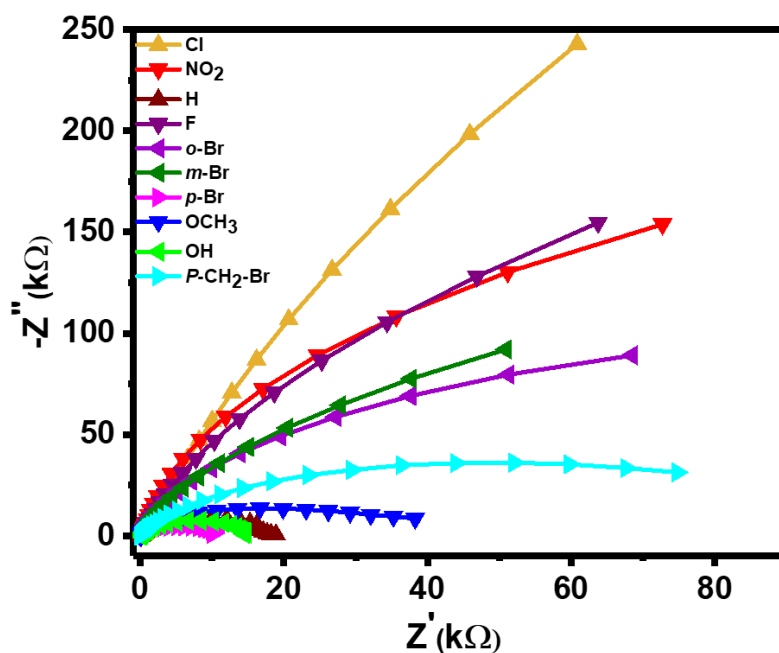


**Figure S10:** Nyquist plot from electrochemical impedance measurement for the AuTP functionalized with different benzene thiol ligands in 0.1M Na<sub>2</sub>SO<sub>4</sub> aqueous solution (pH=7.0) using Ag/AgCl (3.5M KCl) as reference and Pt wire as counter electrode.

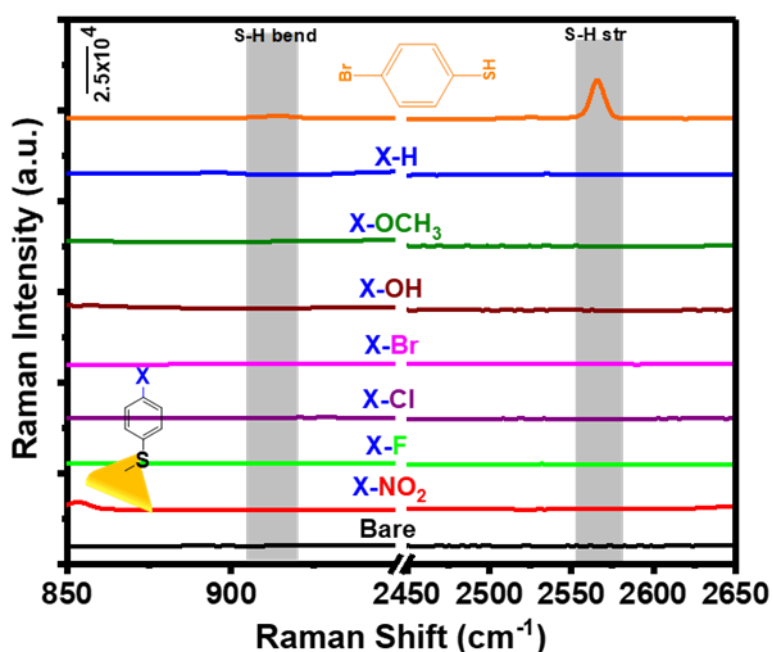


**Figure S11:** SERS analysis of AuTP substrates after each *P*-substituted benzenethiol ligand displayed no S-H stretching (2540-2600 cm<sup>-1</sup>) and S-H bending (~920 cm<sup>-1</sup>) (highlighted above) confirms the binding of the ligand through Au-S bond. The orange spectra (top) correspond to the pure benzenethiol ligand, which displays the S-H stretching mode at 2566 cm<sup>-1</sup> and S-H bending mode at 913.5 cm<sup>-1</sup>, which disappears after attachment to the AuTP surface, confirming the Au-S conjugation.

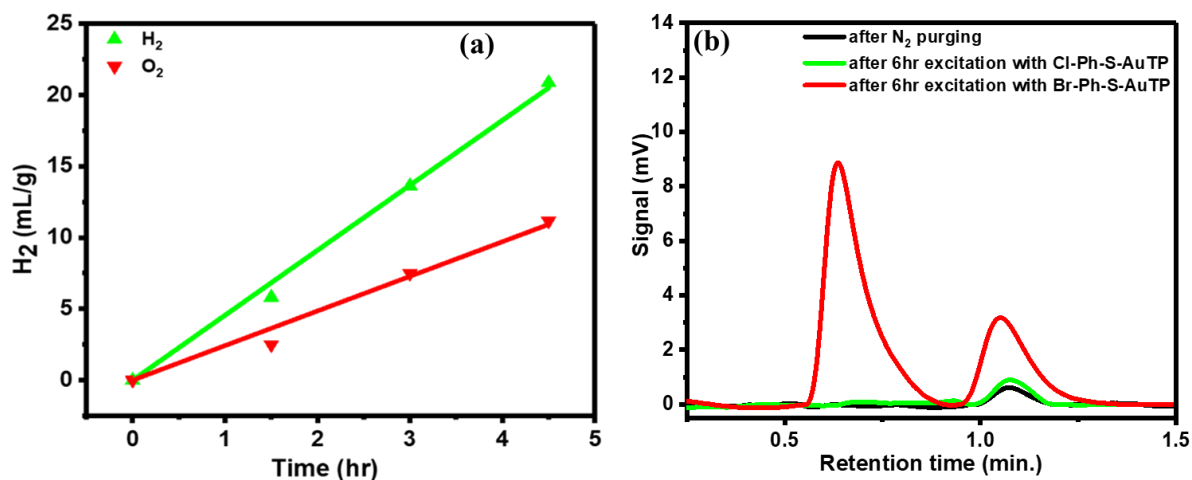


**Figure S12:** (a) The photocatalytic H<sub>2</sub> and O<sub>2</sub> production was observed with 4-Br-Ph-S-AuTP under 808 nm illumination. (b) GC chromatograms were measured before (black) and after 6 hr of 808 nm illumination using 4-Br-Ph-S-AuTP (red) and 4-Cl-Ph-S-AuTP (green) substrate.

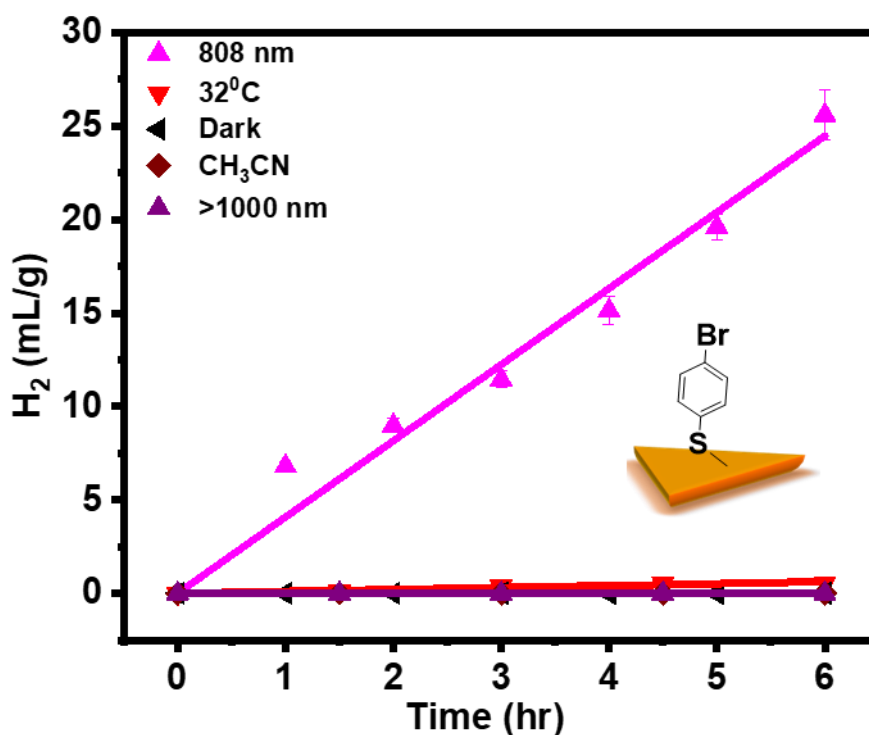


**Figure S13:** Comparison of the H<sub>2</sub> production observed with the 4-Br-Ph-S-AuTP under 808 nm, >1000 nm illumination, at 32°C, under dark, and with CH<sub>3</sub>CN instead of water.

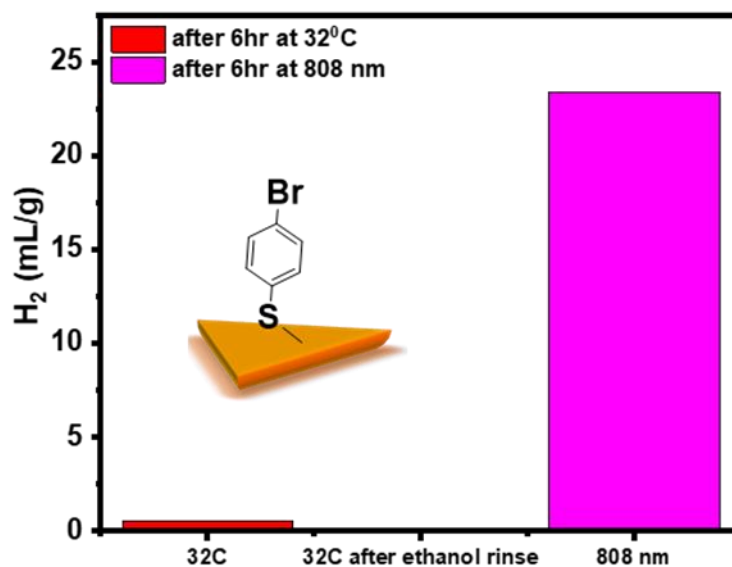


**Figure S14:** Comparison of the H<sub>2</sub> production observed after 6hr with the 4- Br-Ph-S-AuTP at 32<sup>o</sup>C, at 32<sup>o</sup>C after ethanol rinsing, and under 808 nm illumination.

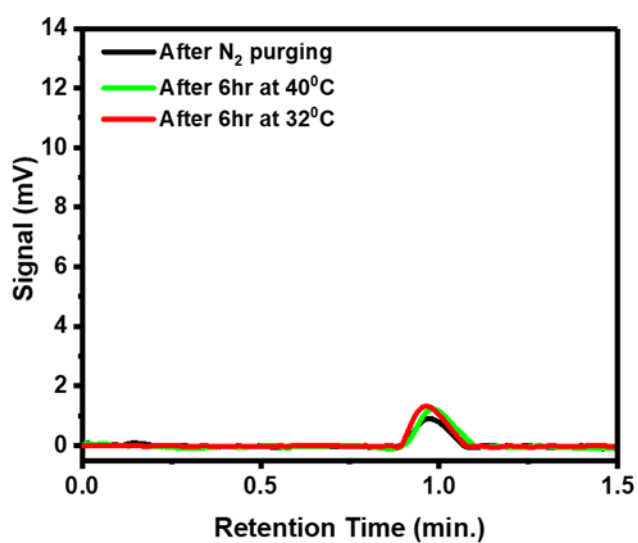


**Figure S15:** GC chromatograms measured after 6 hr with the 4- Br-Ph-S-AuTP at 32<sup>o</sup>C (red) and 40<sup>o</sup>C (green).

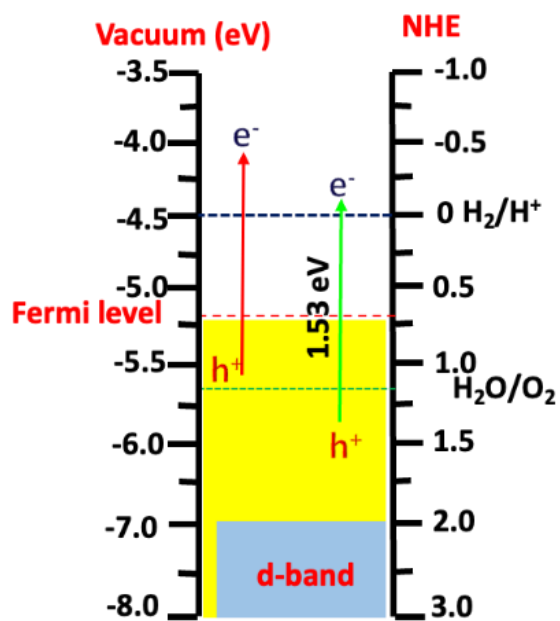


**Figure S16:** An energy diagram showing possible maximum charge-carrier energies in pristine gold nanoparticles under 808 nm excitation.

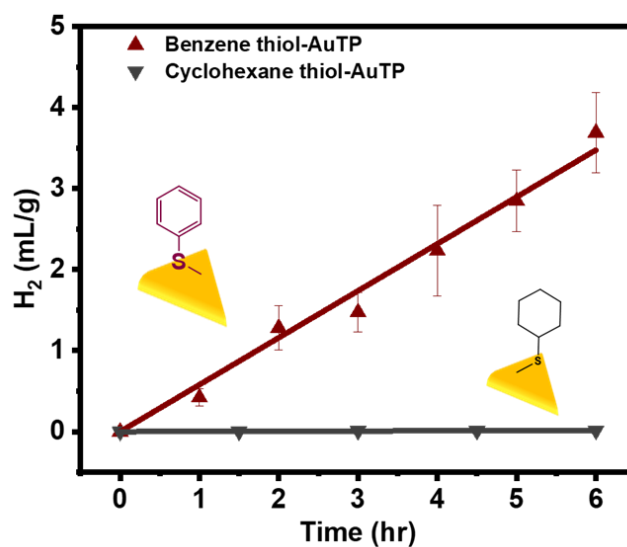


**Figure S17:** Comparison of the photocatalytic H<sub>2</sub> production observed with the benzenethiol-modified AuTP and cyclohexanethiol-modified AuTP photocatalytic substrates.

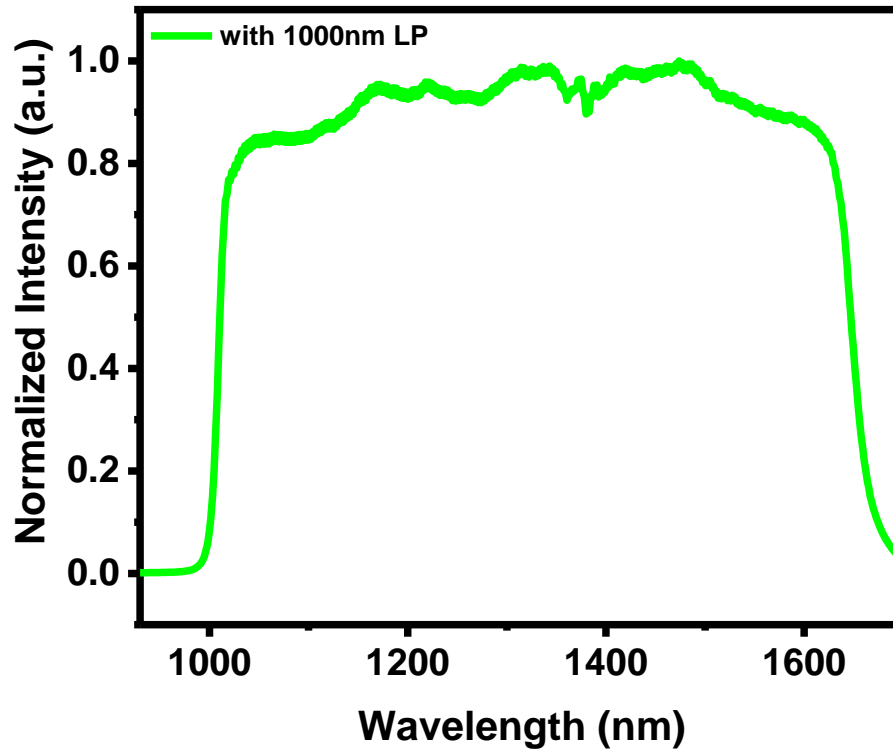


**Figure S18:** Light profile of the white lamp with 1000 nm LP filter.

**Table S1:** The calculated values of charge transfer integral (J), dipole moment ( $D_T$ ) of the Au-ligand systems, and the corresponding  $H_2$  production rate observed through photocatalysis.

<b>Ligand Substitute</b>	<b>J</b>	<b><math>D_T</math></b>	<b><math>D_T^2/J</math></b>	<b><math>H_2</math> (mL/g.hr)</b>
<i>o</i> -Br	0.958045	2.645	7.302397	0.045±0.005
<i>m</i> -Br	0.159014	2.199	30.40991	0.021±0.005
<i>p</i> -Br	0.614732	2.085	7.07174	4.08±0.15
OCH <sub>3</sub>	0.745912	3.004	12.09796	2.92±0.09
OH	0.707738	2.382	8.016984	2.36±0.06
H	0.827239	2.708	8.864746	0.58±0.02
NO <sub>2</sub>	0.143231	1.773	21.94727	0.047±0.003
F	0.272863	1.768	11.45565	0.015±0.002
Cl	0.271414	1.975	14.3715	0.0002±0.0001

## References:

- 1 G. Joshi, A. Saha, A. Dutta and S. Khatua, *ACS Appl. Mater. Interfaces*, 2022, **14**, 38815–38823.
- 2 P. Hohenberg and W. Kohn, *Phys. Rev.*, 1964, **136**, B864–B871.
- 3 W. Kohn and L. J. Sham, *Phys. Rev.*, 1965, **140**, A1133–A1138.
- 4 J. Hutter, M. Iannuzzi, F. Schiffmann and J. VandeVondele, *WIREs Comput. Mol. Sci.*, 2014, **4**, 15–25.
- 5 J. VandeVondele, M. Krack, F. Mohamed, M. Parrinello, T. Chassaing and J. Hutter, *Comput. Phys. Commun.*, 2005, **167**, 103–128.
- 6 J. P. Perdew, K. Burke and M. Ernzerhof, *Phys. Rev. Lett.*, 1996, **77**, 3865–3868.
- 7 C. Hartwigsen, S. Goedecker and J. Hutter, *Phys. Rev. B*, 1998, **58**, 3641–3662.
- 8 S. Goedecker, M. Teter and J. Hutter, *Phys. Rev. B*, 1996, **54**, 1703–1710.
- 9 S. Grimme, J. Antony, S. Ehrlich and H. Krieg, *J. Chem. Phys.*, 2010, **132**, 154104.
- 10 M. J. Frisch et. al., Gaussian 09 Revision E.01. Gaussian Inc. Wallingford CT 2009.
- 11 A. Schafer, H. Horn and R. Ahlrichs, *J. Chem. Phys.*, 1992, **97**, 2571.
- 12 A. Schäfer, C. Huber and R. Ahlrichs, *J. Chem. Phys.*, 1994, **100**, 5829–5835.
- 13 F. Weigend, *Phys. Chem. Chem. Phys.*, 2006, **8**, 1057–1065.
- 14 F. Weigend and R. Ahlrichs, *Phys. Chem. Chem. Phys.*, 2005, **7**, 3297–3305.
- 15 A. D. Becke, *J. Chem. Phys.*, 1998, **109**, 2092–2098.
- 16 J. P. Perdew, *Phys. Rev. B*, 1986, **33**, 8822–8824.
- 17 C. Lee, W. Yang and R. G. Parr, *Phys. Rev. B*, 1988, **37**, 785–789.
- 18 Brown's Open Access Toolset BOAT, [https://joshuasbrown.github.io/docs/CATNIP/catnip\\_home.html](https://joshuasbrown.github.io/docs/CATNIP/catnip_home.html), (accessed May 25, 2023).